Iran Polym J
DOI 10.1007/s13726-017-0570-9

ORIGINAL PAPER

Viscoelastic changes in chlorinated butyl rubber modified with graphene oxide

Ping Jiang[1] · Chunhua Yang[1] · Xianru He[1] · Alisson M. Rodrigues[2] · Rui Zhang[3]

Received: 2 March 2017 / Accepted: 9 October 2017
© Iran Polymer and Petrochemical Institute 2017

Abstract The glass–rubber transition region in multiple component systems is significant for studying the slow relaxation processes in amorphous polymers. It is the first time that graphene oxide (GO) is added into chlorinated butyl rubber (CIIR) to study the effect of GO on different relaxation processes of CIIR. We aimed to give a possible insight to the molecular relaxation behaviors of CIIR/GO nanocomposites. In this study, GO was synthesized by a revised Hummers method, and it was incorporated with CIIR at different contents of 0, 1, 2, 3 and 5 phr (parts per hundred rubber). The structure of GO and CIIR/GO nanocomposites was studied by Fourier transform infrared spectroscopy (FTIR), X-ray diffraction (XRD), attenuated total reflectance-Fourier transform infrared (ATR-FTIR), scanning electron microscopy (SEM) and transmission electron microscope (TEM). Bound rubber was adopted to study the interfacial interaction between GO and CIIR. Differential scanning calorimetry (DSC) and dynamic mechanical analysis (DMA) were also performed. Since there were many conflicting results on the effect of nanoparticles in relation to the glass transition temperature (T_g) of polymer matrixes in correlative literature, we investigated the effect of GO on that of CIIR. The T_g determined by DSC shows slight shifting. However, the maximum and the shoulder of tan δ both shift to low temperatures. In addition, GO increases the coupling effect of CIIR, resulting the shoulder merged with the maximum. A mechanism, though still needs to be further refined, has been proposed to interpret the contradictory results in our case.

Keywords Glass–rubber transition · Segmental dynamics · Chlorinated butyl rubber · Graphene oxide · Slow relaxation processes

Introduction

Research works on glass–rubber transition are not only of great scientific importance but of practical interest for the development of damping materials. However, there are still open issues in the theoretical and experimental fields on this subject [1]. In glass–rubber transition region, the segmental dynamics modes change from local segmental motions (α processes) to slow relaxation processes (α' processes). The first mode is well known as the glass transition, while the latter is not totally understood since 1953 [2]. Ngai et al. [3, 4] proposed the coupling model to explain the thermorheological complexity in glass–rubber transition region, and they indicated that glass–rubber transition region consists of at least three segmental dynamics modes, namely, local segmental motion, Rouse mode, sub-Rouse mode. As described by coupling model, Rouse mode (motion of sub-molecular Gauss chains) and sub-Rouse mode (motion of those units which are longer than segments and shorter than sub-molecular Gauss chains) compose the slow relaxation processes (α' processes) [5]. Some relevant studies showed that different modes have different responses to external factors, such as temperature and frequency. These phenomena are ascribed

✉ Xianru He
xrhe@swpu.edu.cn

[1] State Key Laboratory of Oil and Gas Reservoir Geology and Exploitation and School of Materials Science and Engineering, Southwest Petroleum University, Chengdu 610500, China

[2] Vitreous Materials Laboratory, Department of Materials Engineering, Federal University of São Carlos, UFS Car, São Carlos 13565-905, Brazil

[3] Institut für Physik, Universität Rostock, 18051 Rostock, Germany

Published online: 17 October 2017

to different qualities of these motions [6, 7]. For many amorphous polymers, this property has been verified by dynamic light scattering [8], low-frequencies mechanics spectra [9] and two-dimension analysis [10–12], etc.

The segmental dynamics of many-body systems, such as colloids systems [13, 14], hydrogel [15], polymer blends [16–19] and polymer composites [20], are a new field for studying the nature of glass–rubber transitions [21, 22]. The segmental dynamics of polymer composites has become a hot topic in the past few years. Because of its multiple components, polymer composites often display different properties in the experiments [23]. As a significant carbon material, GO has attracted great attention. However, the effect of GO on the glass transition temperature (T_g) of amorphous polymers is still complex. Wu et al. [24] reported that GO could increase the physical cross-link points which results in higher molecular interaction, so the T_g of natural rubber (NR)is increased. This is well fitted to the result of GO/NR nanocomposites reported by Zhan et al. [25]. However, Liao et al. [26] suggested that the T_g of nanocomposites containing graphene or graphene oxide could be reduced if there was no strong interaction between fillers and polymer matrixes. In addition, a conclusion based on summarizing references in Liao's work was that GO had no influence on T_g of polymers when mixture method was a solution mixture method. A recent master thesis also indicated that GO decreased T_g of polybenzoxazine and polyether ether ketone [27]. This enables us to suspect the universality of the conclusion which was acquired by studying GO/natural rubber nanocomposites [25].

In this study, we incorporate GO into CIIR to study the effect of GO on different segmental dynamics modes. CIIR is a derivative of polyisobutylene, and it has similar segmental dynamics with natural rubber and butyl rubber. As described by coupling model, strong coupling effect often leads to the merging of different segmental dynamics modes. Because CIIR has chlorine side groups, the coupling effect of CIIR is slightly higher than that of natural rubber and butyl rubber. However, chlorine side groups cause better interaction between GO and CIIR than that between GO and other two rubber products. The strong interaction is contributive to the dispersion of fillers in polymer matrixes. In addition, the coupling effect in CIIR is much lower than poly(methyl methacrylate) (PMMA) [9, 12, 23], so the change of its segmental dynamics should be more obvious than that in PMMA. On the whole, CIIR is very suitable for investigating the effect of fillers on different segmental dynamics in the glass–rubber transition region. To the best of our knowledge, GO has not been incorporated into CIIR, a rubber with remarkably slow relaxation processes (α' processes). Investigations of the glass–rubber transition region of CIIR/GO nanocomposites would benefit both academic study and damping materials manufactures [22].

GO is prepared by revised Hummers method [28] at first. Then, GO/CIIR nanocomposites are prepared by solution mixture method. The structure of GO and CIIR/GO nanocomposites is studied by Fourier transform infrared spectroscopy (FTIR), X-ray diffraction (XRD), Attenuated total reflectance-Fourier transform infrared (ATR-FTIR), scanning electron microscopy (SEM) and transmission electron microscope (TEM). In addition, bound rubber is adopted to study the interfacial interaction between GO and CIIR. The segmental dynamics in the glass–rubber transition region of GO/CIIR nanocomposites is characterized by differential scanning calorimetry (DSC) and dynamic mechanical analysis (DMA). In the end, an alternative explanation has been proposed to interpret the results observed in our case.

Experimental

Materials

A commercially available CIIR (Exxon 1068) with a chlorination concentration of 1.26 wt% was purchased from by Exxon Corp. (USA). Natural graphite and *N,N,N′,N′*-tetramethyl-ethylenediamine (TMEDA, > 99.5%) were purchased from Sigma-Aldrich Corp., (USA). *N,N*-Dimethyl formamide (DMF, 99%), tetrahydrofuran (THF, 99%), concentrated vitriol (H_2SO_4) (98%), sodium nitrate ($NaNO_3$), potassium permanganate ($KMnO_4$), hydrogen peroxide (H_2O_2) (35%), zinc oxide (ZnO) and hydrochloric acid (HCl) (36%) were taken from Chengdu Kelong Chemical Corp. (China). Bromomethyl-*p*-tert-octyl phenol formaldehyde resin (trade name PF201) was purchased from Jinan Xinyuan Chemical Corp. (China). It is widely used as the vulcanizing agent of CIIR.

Preparation of GO and nanocomposites

Graphene oxide (GO) was synthesized through a revised Hummers method [28]. In the first step, 230 mL of concentrated H_2SO_4 was added into a 1000 mL tri-necked round-bottom glass reactor. The glass reactor was placed in ice. When the temperature of H_2SO_4 was decreased below 5 °C, 10 g of graphite and 5 g of $NaNO_3$ were introduced into concentrated H_2SO_4 solvent with electric stirring speed of 500 rpm. Furthermore, 30 g of $KMnO_4$ was added into the reactor in six portions for 1.5 h. After addition of $KMnO_4$, the electric stirring was kept about 1 h with constant speed at 35 °C. In the next step, 460 mL of ultra-pure water was slowly added into the reactor. Then, the reaction temperature was adjusted to 95 °C for another 15 min. After that, the mixture solution was transferred into a 5000 mL glass bulk and a certain amount of H_2O_2, to terminate the reaction, was dropwise added into solution until the color of the mixture turned into yellow. The

hydrochloric acid (HCl) was added to dissolve the undissolved substances. Finally, the ultra-pure water was used to wash the products with centrifuging processes until the pH reached about 7. Then, the freeze drying method was adopted to remove water and consequently the graphite oxide was obtained.

GO/CIIR nanocomposites were prepared through solution mixture method. At first, the graphite oxide with designed mass was mixed with TMEDA at a ratio of 1 mL of TMEDA per 1 g of graphite oxide. Then, the mixture was dispersed in 200 mL of DMF. An ultrasonic exfoliation step was conducted on ultrasonic cell smash (JY-90-II, Lingbo Xinzhi Bio-tech. Corp., China) at a working power of 300 W, and graphene oxide (GO) could be obtained after the exfoliation of graphite oxide. An amount of 50 g of CIIR was dissolved into 1000 mL of THF. Finally, the CIIR/THF solution and the GO/DMF suspension solution were mixed about 2 h through high-speed stirring (1000 rad/min). When it was well mixed, the solvent of mixture solution was removed by the reduced pressure distillation method, followed by a 2 days vacuum drying at the temperature of 40 °C. Consequently, a compound of CIIR and GO could be obtained.

The compounds of CIIR and GO were mixed with PF201 and ZnO using a two-roll mill and subsequently subjected to compression at 160 °C for 30 min. The main compound formulation is shown in Table 1. The obtained sample sheets were cut into specified shapes for characterizations.

Characterization

Fourier transform infrared spectroscopy (FTIR) was carried out on Nicolet 6700 (Thermo Fisher Scientific Corp., USA), and potassium bromide (KBr) was mixed with GO to prepare the sample.

X-ray diffraction (XRD) was performed on XPert PRO MPD (PANalytical Corp., The Netherlands) at a generator voltage of 35 kV and a generator current of 25 mA. The scanning range was from 5° to 70°, and the scanning speed was 3.6°/min. The interlayer distance (*d*-spacing) was estimated by Bragg equation, as follows:

$$2d \sin\theta = n\lambda \tag{1}$$

Table 1 The compound formula

Ingredient	Weight (g)
The compound[a]	variable
PF201	1.5
ZnO	1

[a] The compound, consisting of 50 g of CIIR and designing mass of GO (1 phr, 2 phr, 3 phr, 5 phr) was obtained from solution blending

where $\lambda = 1.54$ Å, which is the wavelength of X-ray; $n = 1$, by a series of diffraction; d is the interlayer spacing.

Attenuated total reflectance-Fourier transform infrared (ATR-FTIR) spectra of CIIR/GO nanocomposites were recorded using a Thermo Fisher Scientific Nicoleti S50 attenuated total reflectance-IR spectrometer (Thermo Fisher Scientific Inc., USA) over a wavenumber range of 4000–650 cm^{-1} with solution of 4 cm^{-1}.

The method to determinate the bound rubber was similar to previous reports [29, 30]. Small pieces of less than 0.2 g of CIIR/GO nanocomposite in un-cured state were cut and put into a basket. The basket was immersed into 150 mL of toluene for a week at room temperature. Subsequently, the samples were dried for 1 day at 105 °C. The bound rubber was calculated by the following equation:

$$\mathrm{BdR} = \frac{(m_2 - m_1) - \frac{\mathrm{CPD}}{100}(m_2 - m_3)}{(m_2 - m_1)} \times 100 \tag{2}$$

where m_1 is the mass of the empty basket; m_2 is the mass of the basket plus the unextracted sample; m_3 is the mass of the basket plus the extracted sample; CPD is the total formulation (phr). Each CIIR/GO nanocomposite was tested five times, and the value of bound rubber was calculated by taking the average.

The morphology of the GO/CIIR nanocomposites was studied by scanning electron microscopy (SEM) (Zeiss EV0 MA15, Carl Zeiss Microscopy Corp., Deutschland). To prepare samples for SEM analysis, the nanocomposites were quenched in liquid nitrogen and cryogenically fractured. Before conducting the test, these samples were sputtered with gold.

Transmission electron microscope observations (TEM) were made to study the micro-morphology of GO slices and CIIR/GO nanocomposites. The morphology of GO slices was studied by TEM Libra 200 (Carl Zeiss Corp., Deutschland) under an acceleration voltage of 200 kV. The micro-morphology of CIIR/GO nanocomposites was studied by Tecnai G2 F20 S-TWIN (FEI Corp., USA) under an acceleration voltage of 200 kV. Ultra-thin sections of the specimens were cut at − 100 °C using Leica Ultracut-R ultramicrotome. The copper grids were used to support the GO powder and the thin slices of CIIR/GO nanocomposites.

Dynamic mechanical analysis (DMA) was carried out on Q800 (TA Instruments, USA) by using a dual cantilever clamp and a testing method of temperature step-frequency sweep. The testing frequency was 1 Hz.

Differential scanning calorimetry (DSC) test was performed on a Q20 calorimeter (TA Instruments). The sample was heated isothermally at 40 °C for 5 min, then cooled towards − 70 °C at a cooling rate of 10 °C/min and

stabilized for 5 min. A heating process at a heating rate of 10 °C/min to 40 °C was performed. The glass transition temperature (T_g) was determined as the midpoint of glass–rubber transition region of the heat flow curve.

Results and discussion

The FTIR spectra of the graphite oxide, graphene oxide and the natural graphite are shown in Fig. 1. The difference of the peak intensity between these spectra indicates that the natural graphite is highly oxidized by strong oxidants, namely, H_2SO_4, $KMnO_4$, etc. The broad peaks (dual-peak structure) around 3413 and 3140 cm^{-1} and the peaks (single-peak structure) around 1399 cm^{-1} correspond to the deformation vibration of O–H. Furthermore, the bands at 1625 and 1620 cm^{-1} correspond to the stretching vibration of C=O [27]. The bands at 1115 and 1121 cm^{-1} originate from the C–O stretching vibrations [31]. As described above, the existence of carboxylic acid groups on the surface of graphite oxide and graphene oxide is verified. In addition, the peak at 2344 cm^{-1} is caused by C=O stretching vibration of carbon dioxide (CO_2), which cannot be observed in the natural graphite and graphite oxide curves. The reason is that CO_2 could be easily absorbed on the surface of GO [31–33]. This result indicates the success of peeling and oxidizing procedures.

Figure 2 shows the XRD results of natural graphite and graphene oxide. A sharp peak at 2θ of 25.7° (corresponding to the *d*-spacing of 0.34 nm) can be observed in curve '*a*', which could be ascribed to a typical diffraction plane peak (0 0 2) of natural graphite. When natural graphite was peeled to GO by ultrasonic exfoliation step, the peak intensity was reduced drastically and a new diffraction peak was obtained at 2θ = 11.8° in curve 'b'. The new diffraction peak corresponds to (0 0 1) plane with an interlayer distance of 0.75 nm. XRD results of CIIR/GO nanocomposites are shown in Fig. 3. There are typical diffraction peaks for all CIIR/GO nanocomposites at about 9.4°, which corresponds to the *d*-spacing of 0.94 nm. The diffraction peaks should be ascribed to GO in nanocomposites. Compared with the intrinsic *d*-spacing of GO, the *d*-spacing of GO in nanocomposites increases, which indicates that CIIR molecule might fill in GO interlayer spacing.

Generally, there are two dominating interaction effects between fillers and polymer matrixes, namely, chemical interaction and physical interaction. CIIR/GO

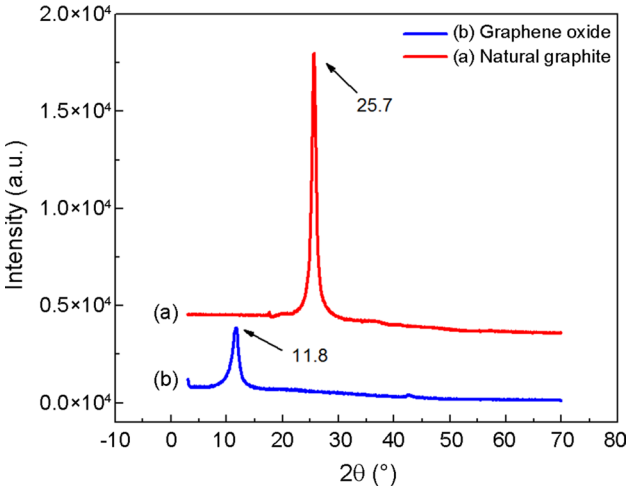

Fig. 2 XRD patterns of natural graphite (**a**) and graphene oxide (**b**)

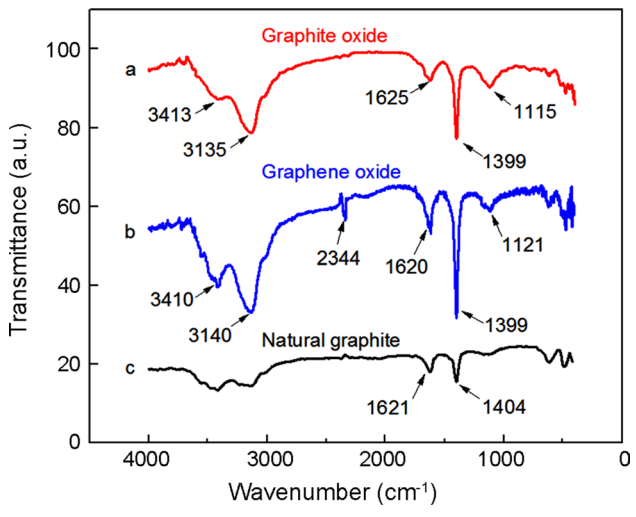

Fig. 1 FTIR spectra of graphite oxide (**a**), graphene oxide (**b**), and natural graphite (**c**). For comparison, the spectra have been shifted vertically only

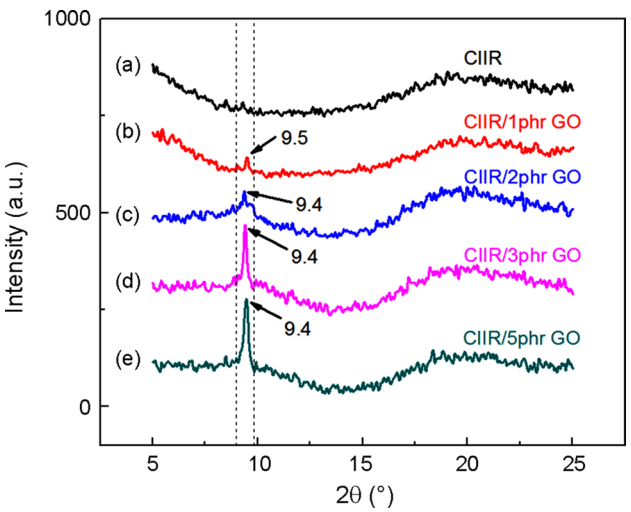

Fig. 3 XRD patterns of CIIR/GO nanocomposites: **a** CIIR, **b** CIIR/1 phr GO, **c** CIIR/2 phr GO, **d** CIIR/3 phr GO, and **e** CIIR/5 phr GO

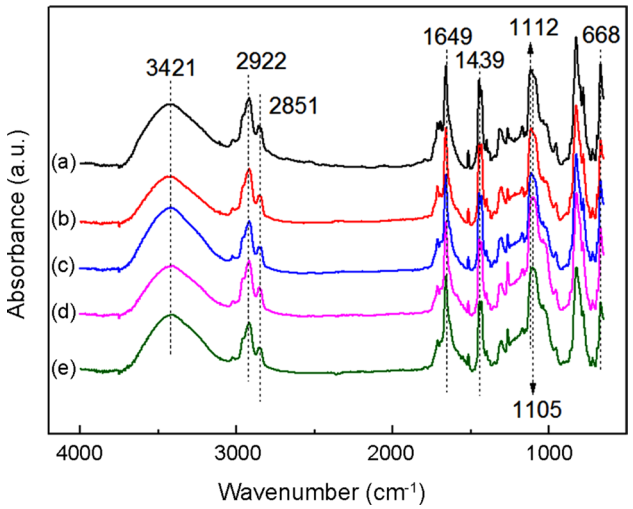

Fig. 4 FTIR-ATR spectra of CIIR and its nanocomposites: **a** CIIR, **b** CIIR/1 phr GO, **c** CIIR/2 phr GO, **d** CIIR/3 phr GO, and **e** CIIR/5 phr GO

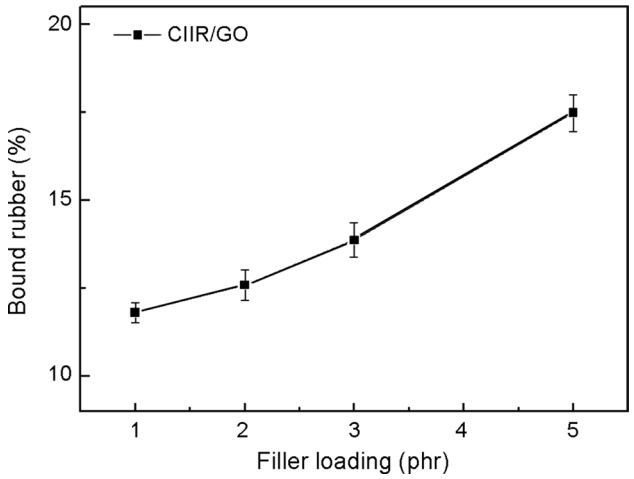

Fig. 5 Bound rubber content of CIIR/GO nanocomposites

nanocomposites are investigated by ATR-FTIR, as shown in Fig. 4. Peaks at around 3421 and 1439 cm^{-1} correspond to the deformation vibration of O–H. The band at around 1649 cm^{-1} corresponds to stretching vibration of C=O. The band at 1112 cm^{-1} refers to the stretching vibrations of C–O. The bands at about 2922 and 2851 cm^{-1} are assigned to the stretching vibration of C–H of methylene groups. The band at 668 cm^{-1} corresponds to the stretching vibration of C–Cl [34]. A slight red shifting of the band at 1112 cm^{-1} could be observed. Especially, after adding 3 phr GO and 5 phr GO, the band shifts to 1105 cm^{-1}. The bands of stretching vibrations of C–O are determined for CIIR, CIIR/1phr GO nanocomposite, CIIR/2phr GO nanocomposite, CIIR/3phr GO nanocomposite, and CIIR/5phr GO nanocomposite at 1112, 1110, 1110, 1105 and 1105 cm^{-1}, respectively. Generally, the change of the wavenumber is attributed to the physical interaction (hydrogen bond, etc.). In addition, no other characteristic peaks are observed with introducing GO into CIIR. Thus, the interaction between GO and CIIR could be mainly ascribed to the physical interaction.

In order to further investigate the physical interaction between GO and CIIR, the quality of interphase was analyzed by bound rubber, related to the amount of rubber molecules absorbed onto fillers. It is widely used to evaluate the interaction between fillers and polymer matrixes [29]. As shown in Fig. 5, the value of bound rubber is at about 10–20%. With increasing GO loading, the bound rubber of CIIR/GO nanocomposites gradually increases. Due to the organic groups on the surface of GO and the large surface area, some molecules of CIIR would be absorbed onto GO. The increment of bound rubber is mainly resulted from the increasing of GO loading. Furthermore, the favorable dispersion state of GO in CIIR would make rubber molecules efficiently absorbed onto GO surfaces.

In Fig. 6, the morphology of GO/CIIR nanocomposites with different GO loadings was studied by SEM. The width of GO slices is at micron order and the thickness of GO is nanoscale, resulting in large surface area. There is no apparent agglomeration of GO with increasing GO loading. In Fig. 6d, a single GO slice in CIIR matrices was observed by SEM. The phase interface between CIIR and GO is ambiguous. The results are ascribed to favorable compatibility between GO and CIIR. In addition, a curly structure of GO was observed in Fig. 6d. This structure could further increase the surface area, so that more rubber molecules could be absorbed onto GO surfaces.

Both GO and CIIR/GO nanocomposites were studied by TEM. As shown in Fig. 7a, the width of GO slices is at micron order and the thickness of the edge is thinner than the central. The curly structures at the edge of GO could also be observed. In Fig. 7b, GO is finely dispersed in CIIR and appears as individual particles. The interface between GO and CIIR is ambiguous, which is the same as the results of SEM. In Fig. 7b, even though the thickness of GO slices is not in the uniform size, the thickness of all GO slices is less than 100 nm. This would provide enough surface area and energy to absorb rubber molecules.

In order to investigate the effect of GO on the glass transition temperature (T_g) of CIIR, DSC has been performed. In Fig. 8, the T_g of nanocomposites is determined by the midpoint of glass–rubber transition region and the value is shown on the right side of thermograms. As shown, the T_g of nanocomposites moves slightly towards lower temperature with GO loading increasing. The onset temperature is also determined and the value is shown on the left side of thermograms. The maximum reduction of T_g and the onset temperature is about 1 K. In addition, the heat capacity of

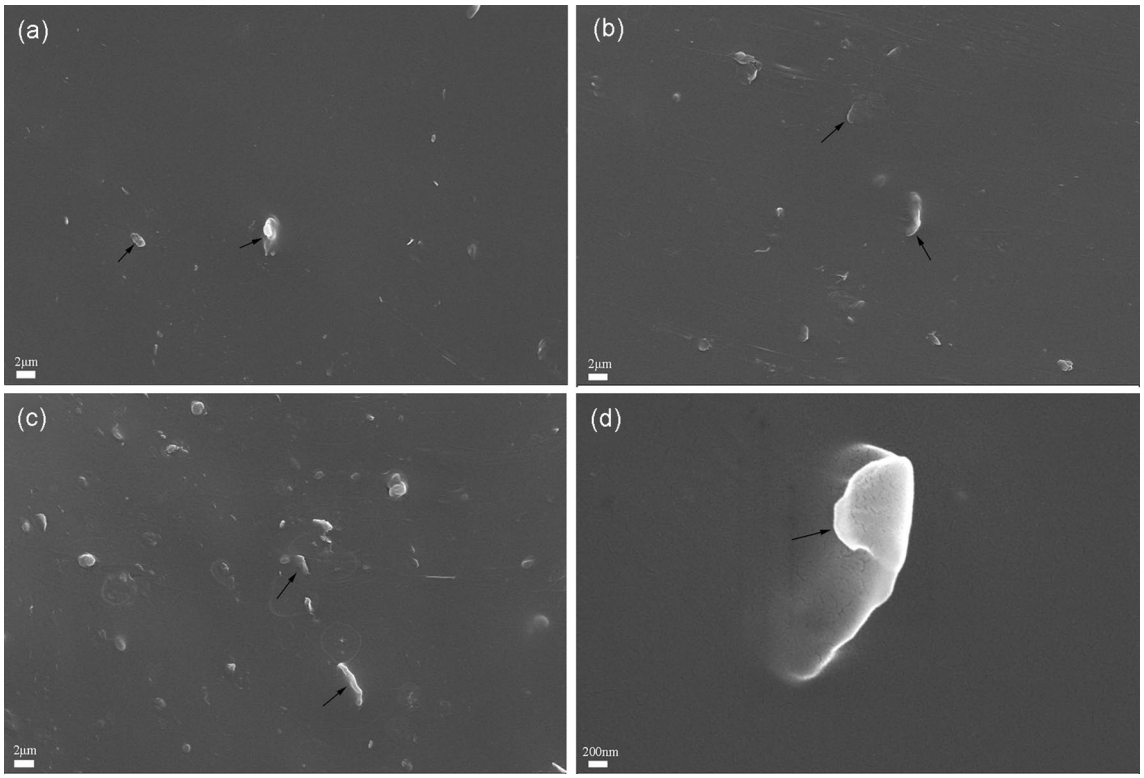

Fig. 6 Morphology of CIIR/GO nanocomposite studied by SEM: **a** CIIR/1 phr GO, **b** CIIR/3 phr GO, **c** CIIR/5 phr GO, **d** single GO slice in CIIR matrixes observed with high amplification

CIIR and its nanocomposites is obtained by analyzing DSC results, as shown in Table 2. With increasing GO loading, the heat capacity, Δc_p, reduces gradually. Furthermore, the immobilized polymer, χ_{im}, could be acquired by the following equation [35]:

$$\chi_{im} = 1 - \frac{\Delta c_p}{\Delta c_p^0 \times (1 - w_{GO})} \tag{3}$$

where Δc_p^0 is the heat capacity increment of CIIR and w_{GO} is the weight fraction of GO. The immobilized polymer could be regarded as bound rubber. It is resulted from the attaching rubber molecules onto GO surface and the intercalating rubber molecules into the interlayer space of GO. As presented in Table 2, with increasing GO loading, the immobilized polymer increases, which resembles the results of bound rubber determined by the swelling method.

Because of its excellent sensitivity, DMA has been widely used to study dynamically mechanical properties and segmental dynamics of polymer composites. Storage modulus (E') is an important parameter in designing materials. Generally, the curve of storage modulus shows three different regions, namely, the glassy state, the glass–rubber transition zone and the rubbery state. The storage modulus of CIIR/GO nanocomposites is presented in Fig. 9a. With increasing temperature, the storage modulus gradually decreases. After adding GO into CIIR matrices, the modulus at glassy state and the rubbery state is considerably increased, as shown in Fig. 9b. The results indicate that the dynamically mechanical properties could be reinforced by introducing GO. This is attributed to the favorable compatibility between GO and CIIR and rubber molecules attached on the surface of GO.

As shown in the inset of Fig. 10, the tan δ of blank CIIR displays a dual-peak structure, with a shoulder peak at low temperature side and a maximum peak at high temperature side. The dual-peak structure of blank CIIR has been widely reported in references [2–5, 9–14, 19–23]. The shoulder corresponds to local segmental motions while the maximum corresponds to slow processes (sub-Rouse mode and Rouse mode). In Fig. 10, the shape of tanδ changes into a single-peak structure after adding GO into CIIR. Wu et al. [22] reported that the height of the maximum was suppressed after adding organic montmorillonite into CIIR, and the maximum shifted to lower temperature while the shoulder kept nearly unchanged. In our case, both the maximum and the shoulder of tan δ shift to low temperature side after introducing GO and the maximum of tan δ increases from 1.48 to 2.47. It is obvious that different shifting extension of the maximum and the shoulder results in the vanishing of dual-peak structure.

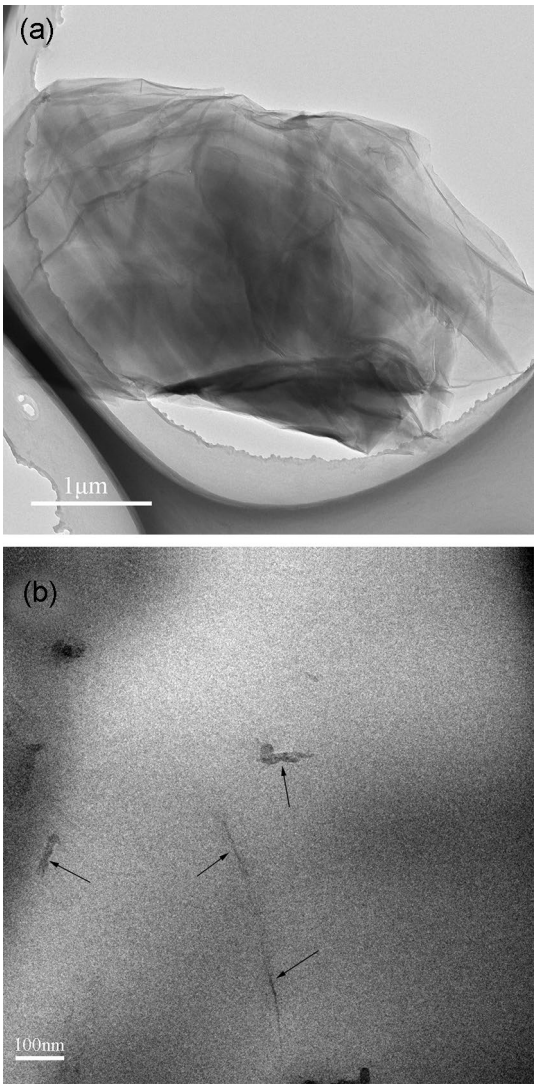

Fig. 7 TEM images of GO (**a**) and CIIR/5 phr GO nanocomposites (**b**)

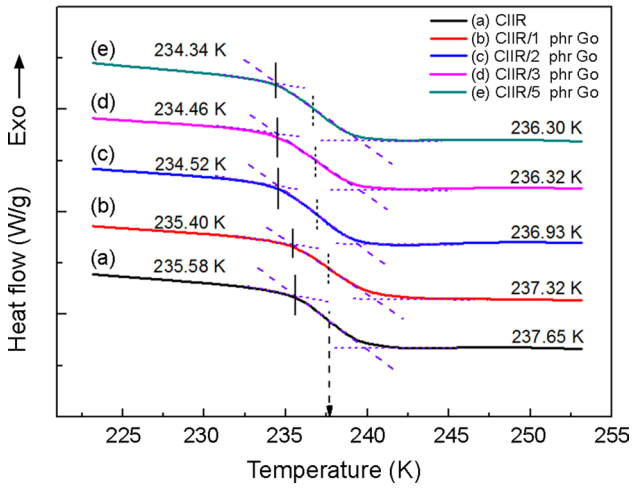

Fig. 8 DSC thermograms of CIIR/GO nanocomposites. For clarity, the thermograms have been shifted vertically only. Each value on the right side of thermograms is the glass transition temperature determined from the thermogram itself; each value on the left side of thermograms is the onset temperature of glass–rubber transition

Table 2 The heat capacity increment and the immobilized polymer of CIIR and its nanocomposites

GO loading/phr	0	1	2	3	5
Δc_p/[J/(g K)]	0.658	0.583	0.573	0.561	0.527
χ_{im}/%	0	10.463	11.15	12.075	15.921

The shifting to low temperature side of the maximum is greater than that of the shoulder, so that the shoulder and the maximum would merge with each other.

The decreasing length of glass–rubber transition region in temperature scale is usually related to strong coupling effects [12]. As described by coupling model, the smaller the coupling effects the greater differences would be observed in temperature or frequency scale between different relaxation modes [3]. To estimate the grade of coupling effects, comparing the breath of normalized loss modulus curves can be used [36–38]. The normalized loss modulus curves of CIIR/GO nanocomposites are in Fig. 11. When the value of G''/G_{max}'' is 0.5, the broadness is represented by B listed in Table 3. The breath of all GO/CIIR nanocomposites (closing to 0.03) is smaller than that of blank CIIR (closing to 0.04). This result suggests that GO increases the coupling effect in CIIR, which might be the reason of the disappeared tanδ dual-peak structure.

Generally, the increasing coupling effect would cause the increasing of the glass transition temperature (T_g). Furthermore, the glass–rubber transition region determined by DSC shares the same molecular motion mechanism with the shoulder determined by DMA [22]. The molecular motion mechanism is usually attributed to the local segments motions. Therefore, the change of T_g determined by DSC and the change in temperature at the shoulder expect to share a similar trend. However, there are some discrepancies in our case. The glass transition temperature of CIIR/GO nanocomposites shifts to low temperature in our case. For qualitative analysis, the T_g determined by DSC and the T_g determined by DMA are decreased. Nonetheless, the extent of reduction in T_g determined by DSC and DMA is different.

In order to interpret the inconsistent results in our case, an alternative mechanism has been proposed. On one hand, because of the strong interaction between CIIR and GO, more physical cross-linked points might form in the CIIR/GO nanocomposites, resulting in increases in coupling effect. Meanwhile, the increasing coupling effect causes the merging of the shoulder (α processes) and the maximum

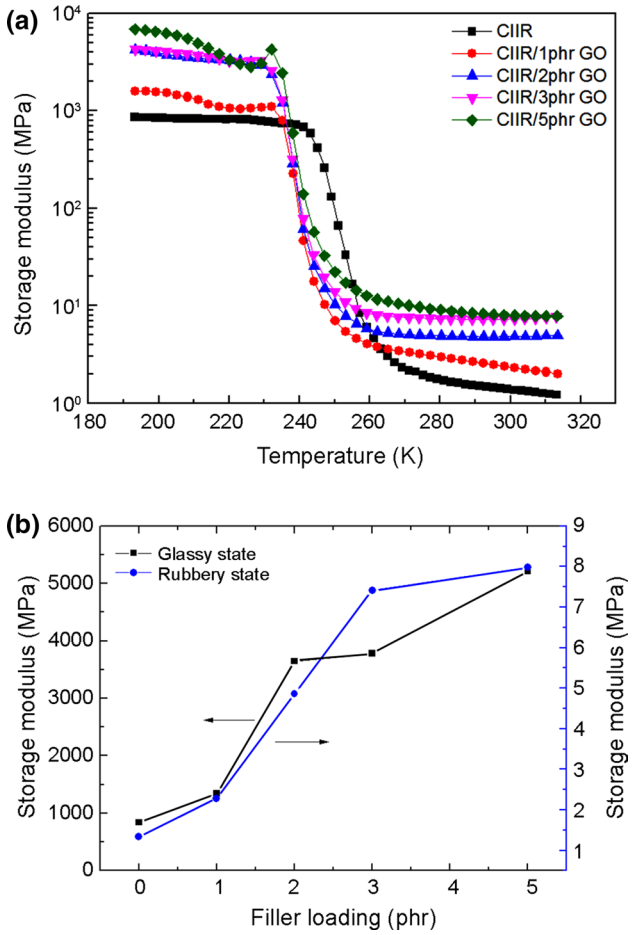

Fig. 9 Storage modulus curves of CIIR and its nanocomposites with different GO contents (**a**) and the plateau modulus (**b**) of glassy state and rubbery state is calculated by taking the average of 195–210 and 290–310 K, respectively

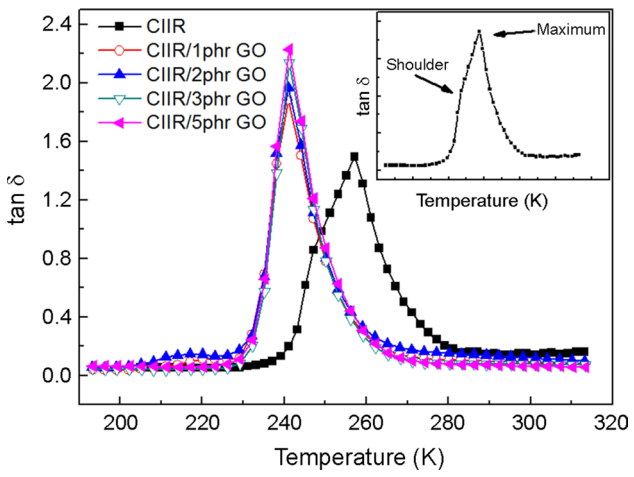

Fig. 10 Tan δ curves of CIIR/GO nanocomposites. The *inset* shows the tan δ curve of blank CIIR, and the black arrows have denoted where the shoulder and the maximum should be

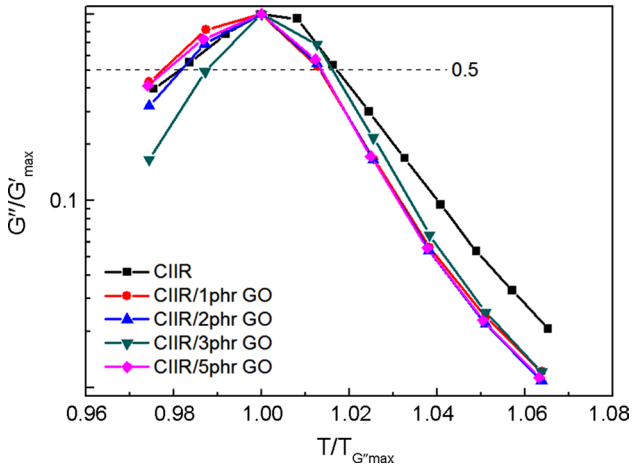

Fig. 11 Normalized loss modulus curves for estimating coupling effect, and G_{max}'' is the maximum in the loss modulus (G'') curve. The dash line indicates the G''/G_{max}'' of 0.5

Table 3 The broadness of normalized loss modulus curves when the value of G''/G_{max}'' is 0.5

Samples (loading of graphene oxide)/(phr)	*B*
0	0.040
1	0.034
2	0.030
3	0.030
5	0.033

(α' processes), resulting in the narrowing peak width of tan δ. On the other hand, GO is a typical two-dimensional layered material. The layered structure is held together by van der Walls interactions. The weak van der Walls interactions between adjacent layers make it possible to form intercalation state or even exfoliation state of fillers. Furthermore, the layer of two-dimensional layered fillers could slip to some extent [39]. For example, Hu et al. [40] prepared reduced graphene oxide/poly(lactic acid) nanocomposites and they identified that the slippage of reduced graphene oxide layers led to the change in poly(lactic acid) resistance. The reason is that the slippage under external forces breaks up the connectivity of conductive networks. In our case, the lamellas of GO are easy to slip horizontally because of the weak van der Walls interaction and the intercalation of rubber molecules into the interlayer space of GO. We describe 'the slippage' as a horizontal and recoverable lamella vibration. A rough schematic diagram is shown in Fig. 12. Even though the slippage of GO lamellae could not result in total change in GO structure, the slippage of lamellae could increase the mobility of polymer chains between two physical cross-linking points, so the glass transition temperatures of CIIR/GO nanocomposites shifts towards low temperature side. In addition, DMA is more sensitive to the effect of structure

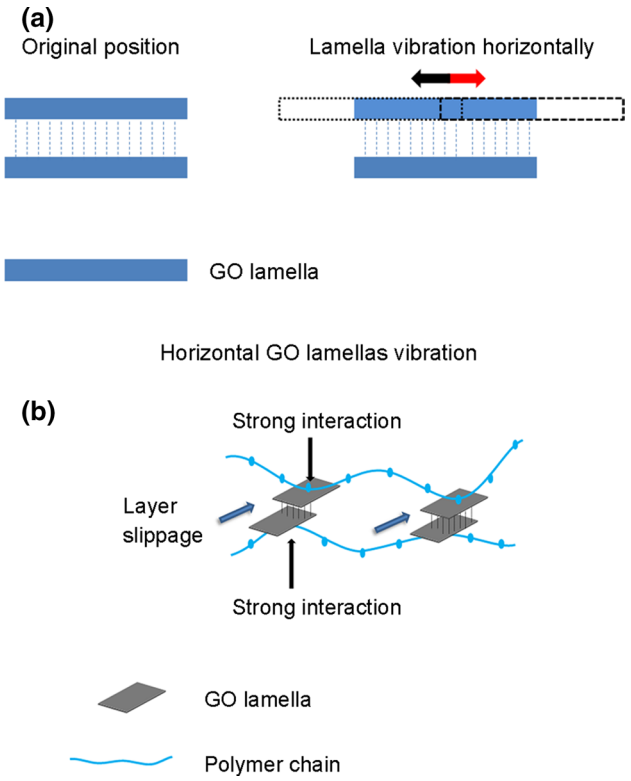

Fig. 12 Schematic diagram of: **a** the motion of GO lamellas and **b** the effect of the lamellae slippage on the mobility of CIIR molecule chains between two physical cross-linked points

vibration of nanocomposites on the glass transition temperature than DSC [41–44]. Consequently, the T_g determined by DMA shifts noticeably to low temperature side and the T_g determined by DSC shows slightly shifted. For qualitative analysis, the T_g determined by both techniques shows a reduction after introducing GO into CIIR. However, there are still questions to be solved. For example, the T_g of CIIR/GO nanocomposites shifts to low temperature side, but the shifting extent is independent of the loading of GO.

Conclusion

In this study, we successfully prepared GO and GO/CIIR nanocomposites. The characteristic bands of GO could be observed in FTIR. TEM results show that the width of GO is at micron order and its thickness is within 100 nm. Based on XRD results of CIIR/GO nanocomposites, the CIIR molecular chains might intercalate into GO. Both ATR-FTIR and bound rubber results show that the interaction between GO and CIIR is physical interaction which results from the organic groups of GO and the large surface area of GO. The favorable compatibility and dispersion state of GO in CIIR matrices, verified by SEM and TEM, improve the dynamically mechanical properties of CIIR/GO nanocomposites. In addition, GO has different effects on the shoulder and the maximum. The shifting to low temperature side of the maximum is greater than that of the shoulder, resulting in the vanishing of the dual-peak structure of tanδ. This is ascribed to the increasing coupling effect which is resulted from the strong interaction between GO and CIIR. However, the recoverable slippage of GO lamellae enhances the mobility of polymer chains between two physical cross-linked points, so that the glass transition temperatures of CIIR/GO nanocomposites shift to low temperature side. It is still a matter that the shifting towards low temperature side of glass transition temperature is independent of the loading of GO, so that the mechanism still needs to be refined and more experiments are envisaged.

Acknowledgements This research was supported by Department of Science and Technology of Sichuan Province (2015JY0052), Open Fund (PLN1429) of State Key Laboratory of Oil and Gas Reservoir Geology and Exploitation (Southwest Petroleum University), Open Fund (X151514KCL22) from Sichuan Province Key Laboratory of Materials for Oil and Gas Industry, and National Counsel of Technological and Scientific Development-Brazil (CNPq-150861/2014-1). The authors appreciate great assistance from Carbontech Corp.

References

1. Gao YY, Wu YP, Liu J, Zhang LQ (2017) Effect of chain structure on the glass transition temperature and viscoelastic property of *cis*-1,4-polybutadiene via molecular simulation. J Polym Sci, Part B: Polym Phys 55:1005–1016
2. Fitzgerald ER, Grandine LD, Ferry JD (1953) Dynamic mechanical properties of polyisobutylene. J Appl Phys 24:650–655
3. Ngai KL (2015) Interpreting the nonlinear dielectric response of glass-formers in terms of the coupling model. J Chem Phys 142:114502
4. Ngai KL, Capaccioli S, Prevosto D (2016) Sub-Rouse modes in polymer thin films: coupling to density and responding to physical aging. AIP Conf Proc 1736:020006
5. Ngai KL (2017) Universal properties of relaxation and diffusion in condensed matter. Chin Phys B 26:018105
6. Glor EC, Angrand GV, Fakhraai Z (2017) Exploring the broadening and the existence of two glass transitions due to competing interfacial effects in thin, supported polymer films. J Chem Phys 146:203330
7. Wang Z, Ngai KL, Wang WH, Capaccioli S (2016) Coupling of caged molecule dynamics to Johari–Goldstein β-relaxation in metallic glasses. J Appl Phys 119:024902
8. Bohdan M, Sprakel J, van der Gucht J (2016) Multiple relaxation modes in associative polymer networks with varying connectivity. Phys Rev E 94:032507
9. Yu WW, Du M, Ye WJ, Lv WY, Zheng Q (2014) Relaxation behavior of layered double hydroxides filled dangling chain-based polyurethane/polymethyl methacrylate nanocomposites. Polymer 55:2455–2463
10. Wang XA, Huang GS, Wu JR, Nie YJ, He XJ, Xiang KW (2011) Molecular motions in glass-rubber transition region in polyisobutylene investigated by two-dimensional correlation dielectric relaxation spectroscopy. Appl Phys Lett 99:121902

11. Jelcic Z, Bulatovic VO, Markovic KJ, Rek V (2017) Multi-fractal morphology of un-aged and aged SBS polymer-modified bitumen. Plast Rubber Compos 46:77–98
12. Zhang R, He XR, Yu H, Chen KY (2014) Detecting the Rouse and Sub-Rouse modes in poly(butyl acrylate) and poly(ethyl acrylate) through two-dimensional dynamic mechanical spectra. J Macromol Sci Part B Phys 53:1642–1653
13. Christie D, Zhang C, Fu J, Koel B, Priestley RD (2016) Glass transition temperature of colloidal polystyrene dispersed in various liquids. J Polym Sci Part B: Polym Phys 54:1776–1783
14. Igwe IE, Zong YW, Yang XN, Ouyang ZC, Chen K (2017) Induced attraction between polystyrene colloidal particles in a binary mixture with PNIPAM colloidal microgels. J Phys Chem B 121:5391–5395
15. Yang M, Liu CY, Zhao KS (2017) Concentration dependent phase behavior and collapse dynamics of PNIPAM microgel by dielectric relaxation [J]. Phys Chem Chem Phys 19:15433–15443
16. Liao FS, Su AC, Hsu TCJ (1994) Damping behaviour of dynamically cured butyl rubber/polypropylene blends. Polymer 35:2579–2586
17. Medjdoub N, Guessoum M, Fois M (2017) Viscoelastic, thermal and environmental characteristics of poly(lactic acid), linear low-density polyethylene and low-density polyethylene ternary blends and composites. J Adhes Sci Technol 31:787–805
18. Chen Q, Zuo M, Yang RQ, Zhang JF, Lv X, Zhang WJ, Song YH, Zheng Q (2017) Evolution of concentration fluctuation during phase separation of polystyrene/poly(vinyl methyl ether) blend in the presence of nanosilica. J Polym Sci Part B: Polym Phys 55:1337–1349
19. Rathika R, Padmaraj O, Suthanthiraraj AS (2017) Electrical conductivity and dielectric relaxation behaviour of PEO/PVdF-based solid polymer blend electrolytes for zinc battery applications. Ionics 1–13
20. Kahar AWM, Sarifuddin N, Ismail H (2017) Structural, thermal and physico-chemical properties of high density polyethylene/natural rubber/modified cassava starch blends. Iran Polym J 26:149–159
21. Zhang R, He XR, Lai ZP, Yang DB (2016) Effect of some inorganic particles on the softening dispersion of the dynamics of butyl rubber. Polym Bull 74:1031–1043
22. Lei ZY, Xing W, Wu JR, Huang GS, Wang XA, Zhao LJ (2014) The proper glass transition temperature of amorphous polymers on dynamic mechanical spectra. J Therm Anal Calorim 116:447–453
23. Zhang R, He XR, Huang GS (2015) A review of the slow relaxation processes in the glass–rubber transition region of amorphous polymers. Phase Trans 2015:843–858
24. Wu JR, Huang GS, Li HX, Wu SD, Liu YF, Zheng J (2013) Enhanced mechanical and gas barrier properties of rubber nanocomposites with surface functionalized graphene oxide at low content. Polymer 54:1930–1937
25. Zhan YH, Wu JK, Xia HS, Yan N, Fei GX, Yuan GP (2011) Dispersion and exfoliation of graphene in rubber by an ultrasonically-assisted latex mixing and in situ reduction process. Macromol Mater Eng 296:590–602
26. Liao KH, Aoyama S, Abdala AA, Macosko C (2014) Does graphene change T_g of nanocomposites? Macromolecules 47:8311–8319
27. Xing YL (2015) The study on the preparation of high-performance polymer nanocomposites and their structure and performance. Southwest Petroleum University, Master Thesis, Chengdu
28. Hummers WS, Offeman RE (1958) Preparation of graphitic oxide. J Am Chem Soc 80:1339
29. Leblanc JL (2002) Rubber–filler interactions and rheological properties in filled compounds. ProgPolym Sci 27:627–687
30. Zou YK, Sun YK, He JW, Tang ZH, Zhu LX, Luo YF, Liu F (2016) Enhancing mechanical properties of styrene–butadiene rubber/silica nanocomposites by in situ interfacial modification with a novel rare-earth complex. Compos A 87:297–309
31. Ganesh BM, Isloor AM, Ismail AF (2013) Enhanced hydrophilicity and salt rejection study of graphene oxide-polysulfone mixed matrix membrane. Desalination 313:199–207
32. Mahmoudi E, Ng LY, Ba-Abbad MM, Mohammad AW (2015) Novel nanohybrid polysulfone membrane embedded with silver nanoparticles on graphene oxide nanoplates. Chem Eng J 277:1–10
33. Olanipekun O, Oyefusi A, Neelgund GM, Oki A (2015) Synthesis and characterization of reduced graphite oxide–polymer composites and their application in adsorption of lead. Spectrochim Acta Part A 149:991–996
34. Pazur RJ, Petrov I (2015) The thermo-oxidation of isoprene containing copolymers of isobutylene: activation energies and reactions from room temperature to 100 °C. Polym Degrad Stab 113:55–65
35. Fragiadakis D, Bokobza L, Pissis P (2011) Dynamics near the filler surface in natural rubber-silica nanocomposites. Polymer 52:3175–3182
36. Zhang R, He XR, Yu H (2014) Why tanδ of poly(butyl acrylate) and poly(ethyl acrylate) with little double bonds are becoming asymmetric? Polymer 55:4720–4727
37. Zhang R, He XR, Huang GS (2014) Dynamics of poly(butyl acrylate) and poly(ethyl acrylate) with internal double bonds. J Polym Res 21:388
38. He XR, Yu H, Zhang R, Yang CH (2014) Enhance slower relaxation process of poly(ethyl acrylate) through internal plasticization. Int Polym Proc 29:419–424
39. Cao FH, Wang JC (2016) Preparation and characterization of hyperbranched polymer modified montmorillonite/chlorinated butyl rubber damping composites. J Appl Polym Sci 133
40. Hu C, Li ZY, Wang YL, Gao JC, Dai K, Zheng GQ, Liu CT, Shen CY, Song HX, Guo ZH (2017) Comparative assessment of the strain-sensing behaviors of polylactic acid nanocomposites: reduced graphene oxide or carbon nanotubes. J Mater Chem C 5:2318–2328
41. Cao J, Wang K, Yang H, Chen F, Zhang Q, Fu Q (2010) Shear-induced clay dispersion in HDPE/PEgMA/organoclay composites as studied via real-time rheological method. J Polym Sci Part B: Polym Phys 48:302–312
42. Zhang R, He XR (2015) Crystallization and molecular dynamics of ethylene-vinyl acetate copolymer/butyl rubber blends. RSC Adv 5:130–135
43. Zhang R, He XR, Yang DB, Lai ZP (2015) Non-isothermal crystallization kinetics and segmental dynamics of high density polyethylene/butyl rubber blends. Polym Int 64:1252–1261
44. Zhang R, He XR, Yu H (2015) Transitions and molecule motions in glass–rubber transition zone of amorphous polymers. Polym Mater Sci Eng 31:186–190